Holocene sea-level change on the central coast of Bohai Bay, China

Fu Wang[1,2], Yongqiang Zong[3], Barbara Mauz[4,5], Jianfen Li[1,2], Jing Fang[6], Lizhu Tian[1,2], Yongsheng Chen[1,2], Zhiwen Shang[1,2], Xingyu Jiang[1,2], Giorgio Spada[7] and Daniele Melini[8]

[1]Tianjin Center of Geological Survey, China Geological Survey (CGS), Tianjin, China
[2]Key Laboratory of Coast Geo-Environment, China Geological Survey, CGS, Tianjin, China
[3]Department of Earth Sciences, The University of Hong Kong, Hong Kong SAR, China
[4]School of Environmental Sciences, University of Liverpool, Liverpool, UK
[5]Department of Geography and Geology, University of Salzburg, Salzburg, Austria
[6]College of Urban and Environmental Science, Tianjin Normal University, Tianjin, China
[7]Department of Science, University of Urbino, Urbino, Italy
[8]Istituto Nazionale di Geofisica e Vulcanologia, Roma, Italy

Correspondence to: Fu Wang (wfu@cgs.cn)

Abstract. To constrain models on global sea-level change regional proxy data on coastal change are indispensable. Here, we reconstruct the Holocene sea-level history of the northernmost China Sea shelf. This region is of great interest owing to its apparent far-field position during the late Quaternary, its broad shelf and its enormous sediment load supplied by the Yellow River. This study generated 25 sea-level index points for the central Bohai coastal plain through the study of 15 sediment cores and their sedimentary facies, foraminiferal assemblages and radiocarbon dating the basal peat. The observational data were compared with sea-level predictions obtained from global GIA models and with published sea-level data from Sunda shelf, Tahiti and Barbados. Our observational data indicate a phase of rapid sea-level rise from c. -17 m to -4 m between c. 10 ka and 5 ka with a peak rise of 6.4 mm/a during 8.7 ka to 7.5 ka and slower rise of 1.9 mm/a during 7.5 ka to 5.3 ka followed by a phase of slow rise from 5 ka to 2 ka (~0.4 mm/a from -3.58 m of 5.3 ka cal BP to -2.15 m of 2.3 ka cal BP). The comparison with the sea-level predictions for the study area and the published sea-level data is insightful: in the early Holocene Bohai Bay's sea-level rise is dominated by a combination of the eustatic and the water load components causing the levering of the broad shelf. In the mid-

late Holocene the rise is dominated by a combination of tectonic subsidence and fluvial sediment load which masks the mid-Holocene highstand recorded elsewhere in the region.

KEYWORDS: Sea level; Holocene; Glacial Isostatic Adjustment; Ice Equivalent Sea Level; Bohai Bay

1. Introduction

The sea-level rise since the mid-19th century is one of the major challenges to humanity of the 21st century (IPCC, 2014). The driving mechanisms of this rise are relatively well-known on a global scale, but on a regional scale the mechanisms are modified by local parameters. One of these parameters is the regional Holocene sea-level history, which is a background sea-level signal of variable amplitude. In fact, the regional response to sea-level changes may be very different from the global signal (Nicholls and Cazenave, 2010), and, understanding regional costal environment is a rising demand of policy makers. Here, we study the Holocene sea-level history of Bohai Sea, which is the northernmost part of China Sea. The area is of special interest because its shoreline is situated on the broad shelf of the East China Sea (Fig. 1) in the far-field of the former ice sheets. While the far-field site should have a sea-level history similar to the ice-equivalent sea level, the broad shelf is thought to affect the sea-level by up to 10 m height (e.g. Milne and Mitrovica, 2008) in a spatially complex manner. For example, only a very minor Holocene highstand was recorded at sites along the southeast and south coast of China (Zong, 2004). In fact, no obvious Holocene highstand was recorded in the Hangzhou Bay (Xiong et al., 2020) and the Pearl River delta (Xiong et al., 2018). In addition, the exceptionally high supply of fine-grained fluvial sediment to the bay should have influenced shoreline migration in the past. In order to reliably constrain the sea-level history in such complex settings, high-resolution proxy data are required and compared with glacio-isostatic adjustment (GIA) model predictions where the difference between model and proxy datum should allow inferring the non-GIA, hence local, impact on the sea-level history. We show here that shelf effect and local processes influence the regional sea-level history at different times.

2. The study area

The study area lies in a mid-latitude, temperate climate zone (Fig. 1a) on the north-western coast of the East China Sea's wide shelf. Geologically, the Bohai Bay is a depression filled by several kilometre-thick Cenozoic sediment sequences with the top 500 m ascribed to the Quaternary (Wang and Li, 1983). The long-term tectonic subsidence has been estimated to about 1.3-2.0 mm/a at Tianjin City (Wang et al., 2003). The Bay is a semi-enclosed marine environment, connected to the Pacific through a gap between the two peninsulas, Liaodong Peninsulas and Shangdong Peninsulas and the Yellow Sea (Fig. 1b). Our study area is the central coast of the Bay which lies between two deltaic plains, the Yellow River delta in the south and the Luan River delta in the north (Fig. 1b). Several small rivers (e.g., Haihe and Duliujianhe, Fig. 1c) cut through the coastal plain and enter the Bay. The coastal lowland is characterised not only by its low-lying nature, (less than 10 m above sea level), but also by a series of chenier ridges situated south of the Haihe River and buried oyster reefs situated north of the Haihe River (Fig. 1c; Li et al., 2007; Su et al., 2011; Wang et al., 2011; Qin et al., 2017). Local reference tidal levels such as mean high waters (MHW) and highest high waters (HHW) are 1.25 m and 2.30 m respectively, based on the four tidal stations on the coast of Bohai Bay (Fig. 1c). During the Last Glacial Maximum the shoreline moved to the shelf break of the Yellow Sea, more than 1000 km to the east and southeast of our study area (e.g., He, 2006). During the Holocene the sea inundated the coastal area with the shoreline moving about 80 km inland (e.g., Wang et al., 2015).

Previous studies focused on the chenier ridges and palaeo-shoreline change of Bohai Bay (Wang, 1964). Subsequently, a series of studies on marine transgression and lithostratigraphy provided the framework for understanding the late Quaternary evolution of Bohai Bay (e.g., Zhao et al., 1979; Fig. S1). Over 130 Holocene sea-level data, generated in the study area since the early 60ths, were recently compiled by Li et al. (2015; Fig. S2; for details see supplement). However, because no correction for compaction was carried out and no screening took place by which unsuitable material (e.g., transported shell) is rejected, the dataset requires further scrutiny and is not used in our study.

3 Methods

3.1 Sampling and elevation measurements

To obtain sedimentary sequences for this study, we consulted previous studies (*e.g.* Cang *et al.*, 1979; Geng, 1981; Wang *et al.*, 1981; Wang, 1982; Yang and Chen, 1985; Zhang *et al.*, 1989; Zhao *et al.*, 1978; Xue et al., 1993) to learn where in the bay marine deposits are dominant and where the landward limit of the last marine transgression should occur. We then collected 15 cores along W-E transects from the modern shoreline to 80 km inland (Fig. 1c), using a rotary drilling corer. Transect A, comprising 6 cores, stretches from the modern shoreline 80 km inland and crosses the inferred Holocene transgression limit (Xue, 1993). Transects B, C and D, comprising 9 cores, cross the transgression limit a little further south (Fig. 1c). The surface elevations of the drilled cores were levelled to the National Yellow Sea 85 datum (or mean sea level, MSL) using a GPS-RTK system with a precision of 3 cm. The GPS-RTK raw data were corrected and processed to National Yellow Sea 85 datum system by the CORS system network available from the Hebei Institute of Surveying and Mapping with National measurement qualification.

3.2 Sediment and peat analyses

In the laboratory, the sediment cores were opened, photographed and recorded for sedimentary characteristics including grain size, colour, physical sedimentary structures, and content of organic material. To study the degree of marine influence in the muddy sediment sequences, sub-samples were collected in 20 cm intervals. These were analysed with respect to diatoms and foraminifera with a subsequent focus on the foraminifera due to poor preservation of diatoms. The foraminifera of the >63μm fraction of 20 g dry sample were counted (e.g., Wang et al., 1985) following studies on modern foraminifera (e.g. Li, 1985; Li et al., 2009). Sediment description followed Shennan et al. (2015): where in the sediment sequences foraminifera first appear and/or significantly increase (from zero or less than 10 to more than 50) is noted as transgressive contact, while the sediment horizon where foraminifera disappear and/or decrease significantly are noted as regressive contact. These changes are often associated with lithological changes, such as from salt-marsh peaty sediment to estuarine sandy sediment or tidal muddy sediment across a transgressive contact, or vice

versa. In addition, peat material was analysed in terms of its foraminifera content so that salt-marsh peat can be differentiated from freshwater peat.

3.3 Analysis of compaction

Because the Holocene marine deposits are mainly unconsolidated clayey silt with around 0.74% organic matter (Wang et al. 2015) post-depositional auto-compaction (Brain et al., 2015) may have led to lowering of the SLIP. According to Feng et al. (1999), the water content and compaction of marine sediments show positive correlation with the down-core reduction of water content of the Holocene marine sediment being about 10%. Based on these observations, we assumed the maximum lowering is about 10% of the total thickness of the compressible sediment beneath each SLIP. Consequently, the total lowering for an affected SLIP is 10% of the total thickness of the compressible sequence beneath the dated layer divided by the post-depositional lapse time proportional to the past 9000 years (e.g. Xiong et al., 2018), i.e. since the marine transgression in the study area.

3.4 Radiocarbon analyses

69 bulk organic sediment samples from salt-marsh peat were collected from drilling cores, and the peat or plant subsamples obtained from these bulk sediments were chosen for AMS radiocarbon analysis at Beta Analytic Inc. because these can give more reliable ages than shells for the SLIPs. The resulting raw radiocarbon ages were converted to conventional ages after isotopic fractionation were corrected based on $\delta^{13}C$ results. The conventional radiocarbon ages were calibrated to calendar years using the data set Intcal13 included in the software Calib Rev 7.0.2 for organic samples, peat and plant samples (Reimer, *et al*., 2013). Because Shang et al. (2018) reported age overestimation of 467 years for the bulk organic fraction of salt-marsh peaty clay compared to the corresponding peat fraction, all the AMS ^{14}C ages between 4000 to 9000 BP obtained from salt-marsh samples were corrected by $Y=0.99X–466.5$ (Y is the corrected age, *X* is the age obtained from the organic fractions; Shang et al., 2018) except one <600 years age from borehole Q7 (Table 1).

3.5 Sea-level index points (SLIPs)

To develop SLIPs, salt-marsh peaty clay layers were used. To convert the dated peat layers into a SLIP, the modern analogue approach was used by measuring the elevation of the modern open tidal flat (Fig. 2) and sampling its surface for their foraminiferal content. Following the studies of the modern foraminifera assemblage (Li, 2009) *Ammonia beccarii* typically occurs in the upper part of an intertidal zone and *Elphidium simplex* in the lower intertidal zone. The zonation of the modern foraminifera assemblage was then used to identify the indicative meaning of the salt-marsh peat layers: the paleo-mean sea level is the midpoint between high water of spring tides (HHW:+2.3 m) and mean high waters (MHW:+1.25 m) which is 1.78 m with ±0.53 m uncertainty (Wang et al., 2012, 2013; Li et al., 2015). For each dated salt-marsh peat layer the indicative meaning and range, the total amount of possible lowering in elevation due to sediment compaction and the reconstructed elevation of palaeo-MSL are listed in Table 1.

3.6 GIA modelling

The time-evolution of sea level was obtained using the open source program SELEN (Spada and Stocchi, 2007) to solve the “Sea Level Equation" (SLE) in the standard form proposed in the seminal work of Farrell and Clark (1976). In its most recent development, SELEN (version 4) solves a generalized SLE that accounts for the horizontal migration of the shoreline in response to sea-level rise, for the transition from grounded to floating ice and for Earth’s rotational feedback on sea level (Spada and Melini, 2019). The programme combines the two basic elements of GIA modelling (Earth’s rheological profile and ice melting history since the Last Glacial Maximum) assuming a Maxwell viscoelastic incompressible rheology. The GIA models adopted are ICE-5G(VM2) (Peltier et al., 2004), ICE-6G(VM5a) (Peltier et al., 2012), both available on the home page of WR Peltier, and the one developed by Kurt Lambeck and colleagues (National Australian University, denoted as ANU hereafter; Nakada and Lambeck, 1987, Lambeck et al., 2003) provided to us by A Purcell (pers. com. 2016). Table S1 summarises the values used for each model. The palaeo-topography has been solved iteratively, using the present-day global relief given by model ETOPO1 (Amante and Eakins, 2009). All the fields have been expanded to harmonic degree 512, on an equal-area icosahedron-based grid (Tegmark, 1996) with a uniform resolution of ~20 km. The rotational effect on sea-level change has been taken into account by adopting the “revised rotational theory” (Mitrovica and Wahr, 2011).

4. Results

4.1 Lithostratigraphy and facies

Lithostratigraphically, the cores show a succession of terrigenous (including fresh-water swamp, river channel, flood plain), salt marsh and marine sediments (Table S2) with a clear W-E trend from terrestrial to marine dominance of deposits (Fig. 3-6). The around 80 km long transect A shows this trend: close to the modern shoreline pre-Holocene terrigenous sediments are overlain by basal peat including salt-marsh peat or peaty clay. Further inland these are replaced by fresh-water peat overlain by salt marsh and intertidal sediments and, above, by terrigenous sediments. The cores DC01, CZ01 and CZ02 are composed of fluvial sediments only, roughly confirming the Holocene maximum transgression inferred by Xue (1993). Multiple shifts between salt marsh, marine and fluvial deposits are noticeable in cores QX02, QX03, CZ61 which originate from the central part of the study area.

Marsh deposits are either a blackish and thin freshwater peat mostly interbedded in yellowish fluvial sediments or a yellowish-brown salt-marsh peat bearing intertidal foraminifera (Table 1). Their lower boundaries are usually sharp, and their upper boundaries are mostly diffused or the salt-marsh peat changes gradually into dark grey intertidal sediments. Salt-marsh peat is intercalated in marine sediment sequences (i.e. QX01, QX02, CZ61, CZ85, CZ66 and CZ03, Fig. 3-6), particularly at sites that are close to the Holocene maximum transgression limit.

4.2 Foraminifera data

Foraminifera were identified in all cores except CZ01, CZ02 and DC01 which originate from the landward site of the maximum transgression limit. As the Fig. 4 and 6 show that, foraminifera start to appear at 11.2 m depth, which is dated to about 7.85 ka cal BP in QX01. Abundance of fossil foraminifera changes from about 404 – 772 individuals per samples at depths from 11.2 m to 10.8 m, 68 – 338 specimens from 9.4 m to 8.8 m, and 103 – 3456 counts from 8.2 m to 7.6 m. The assemblages reach maximum abundance at 6.6 m depth which is dated to between 5.29 and 5.23 ka cal BP, with over 30,000 individuals per sample, before disappearing at 5.6 m. Dominant species change from Nonion glabrum in 11.2 – 7.4 m to Ammonia beccarii vars. in 7.4 – 6.4 m. This change represents a change from a salt marsh to a lagoon. In QX02, the pattern of

foraminifera distributions is very similar. Low numbers of foraminifera, mostly Nonion glabrum, start to appear at about 10.1 m (-6.53 m of sea level), as dated to between 7.87 and 7.49 ka cal BP. The abundance reaches its highest at 6.7 m (-3.13 m of sea level), and the assemblages were dominated by Ammonia beccarii vars. Foraminifera disappears sometime between 5.72 and 3.52 ka cal BP. In all seaward drilling core, CZ03, CZ80, CZ85, CZ66, CZ87, CZ61, CZ65, ZW15 and Q7, the pattern of foraminifer's distributions are very similar as QX01 and QX02 (Fig. 4). The foraminifera start to appear in low numbers in the layer just above the basal peaty clay. This first appearance is in ca. 17-8 m depth dated to 9-7 ka cal BP. Above this depth the count increases from ~100 to ~3000 foraminifera per sample at ca 8-7 m depth. The maximum count with >30,000 individuals per sample is reached at -6-5 m dated to around 5 ka cal BP. Foraminifera disappear in these cores sometime between 5.7 ka cal BP and 3.5 ka cal BP. The foraminifera assemblage is composed of few species only, hence not rich and first dominated by *Nonion glabrum* in 17-7 m depth and then dominated by *Ammonia beccarii* vars.in 7-6 m depth. Other species found are *Quinqueloculina akneriana rotunda* and *Protelphidium tuberculatum* (Figs. 4 and 6).

4.3 Modern analogue and indicative meaning and range

The data obtained from the modern analogue shows that the tidal flat can be divided into two sub-environments: intertidal with bioturbation (worm hole developed in tidal surface) and supratidal with salt-marsh vegetation (Fig. 2). Within the supratidal and salt-marsh zones, the foraminiferal assemblages are dominated by *Ammonia beccarii* covering an elevation range from +1.42 m to +2.00 m, including the +1.79m boundary of salt marsh with plants. At sites below these elevations, i.e. intertidal with bioturbation (Fig. 2), the foraminiferal assemblages are dominated by *Elphidium simplex*, *Ammonia beccarii and Pseudogyroidina Sinensis*. This foraminiferal zone covers an elevation ranging from 1.42 m to modern MSL.

Besides occasional *A.beccarii* there are few living foraminifera in the salt marsh above the MHW. The abundance is either biased towards *Ammonia beccarii* or it is relatively small. The latter is most probably due to the area being situated above the MHW and, hence, subject to evaporation during low tide, with the consequence of a relatively high and highly variable salt content of the pore water in the intertidal zone. The modern analogue samples confirm the bias towards salt-tolerant species (Fig. 2, Table 1). The spatial

distribution of the ages confirms the E-W trend of the Holocene transgression where the oldest age is close to the modern shoreline and the youngest age is close to the maximum transgression limit.

4.4 Sea-Level Index Points

In total 25 sea-level index points were established from the dated basal salt-marsh peat using the information obtained from the modern analogue. In Core Q7, at the most seaward location in the study area, the basal SLIP is dated to ~9700 cal BP (Table 1), marking the onset of marine inundation of the study area. The overlying marine sequence is capped by a thick layer of shelly gravels at 1.30 m depth and the associated SLIP is dated to 540 cal BP. This marks the upper end of the marine sequence as foraminifera start to disappear alongside a change from intertidal to supratidal environmental conditions. The cores ZW15, QX02, QX03, QX01 show the same sequence as Q7 and provide 6 SLIPs. 19 SLIPs were collected from other cores (Table 1).

3. Discussion

5.1 Quality of SLIP data

Owing to elevated and variable salinity of the coastal water samples from both cores and modern tidal flat are characterised by low microfauna diversity and low number of foraminifera species. This precludes the use of transfer function statistics and compels analysis based on direct comparison with the modern environment. We have solved this analytical problem by establishing SLIPs exclusively from basal salt-marsh peat in transgressive contact and by correcting the data for compaction. This analytical rigor allowed generating more accurate and more precise SLIP data than those reported by Li et al. (2015) because these earlier SLIP data are characterised by relatively poor chronological and elevation control (for details see supplement). Notwithstanding SLIP improvement in terms of accuracy and precision, fluctuation of the data exist that can exceed 1 m (e.g. at 3.9 ka and at 5.2 ka, Fig. 7). Although hard to prove due to lack of data, we believe that these fluctuations are caused by groundwater extraction which lowers the surface in places.

5.2 The observed Holocene sea-level rise

The SLIPs established indicate two phases of sea-level rise during the Holocene. The first phase occurred in the early Holocene until ~6.5 ka when the sea level rose from -17 m to -4 m. The second phase occurred from ~6.5 ka to 2 ka when the sea level rose from -4 m to -2 m. The oldest Holocene shoreline in Bohai Bay is, situated at -17.2 m at ~9.7 ka cal BP, similar to Tian et al. (2017) who indicate ~-20 m at 9.4 ka cal BP based on seismic units and drilling cores. Between around 8.8 ka and 7.5 ka cal BP the sea level rose rapidly from -15.4 m to -7.0 m at a rate of ca 6.4 mm/a. Then, from 7.5 ka to 5.2 ka cal BP the relative sea level rose to -3.6 m at an average rate of 1.9 mm/a and to -1.2 m until 3.8 ka cal BP, before falling to -2.1 m at 2.3 ka cal BP with an average rising rate of ca. 0.4mm/a from 5.2 to 2.3 ka cal BP. The final phase from 2 ka to today is constrained by only one SLLP from core Q7 dated to 540 cal BP at ~0.5 m (Table 1). Lithostratigraphic data (Shang et al., 2016) suggest that surface of the intertidal sediment body remained very close to zero m from the landward limit of the marine transgression to about 2 km inland from the present shoreline. Further inland, in borehole ZW15 the surface elevation of the same intertidal sediment body is ~3.0 m lower than in core Q7 (Figs. 3 and 4) suggesting a rise of sea level in Bohai Bay in the last 1000 years.

5.3 Observed and predicted Holocene sea level

We compare our observational data with GIA models employed in this study and with Bradley et al. (2016; henceforth denoted as BRAD; see also Table S1) who examined several ice-melting scenarios together with a range of Earth-model parameters, and validated model outputs using published SLIP data from East China Sea coast including Bohai Bay.

Figure 7a displays observational data and sea-level predictions generated in this study. It shows that none of GIA models approximates the observations. The difference ranges between around 14 m at 9 ka and 3 m at 2.5 ka. Bohai Bay's oldest Holocene shoreline (~9.7 ka cal BP) is at -17.2 m (observed), at ca – 35 m (ANU) or at ca -10 m (ICE-X). The BRAD model predicts this shoreline to be at ~-20 m at 10 ka. Our observed shoreline elevation is similar to Sunda Shelf (ca -15 m; Hanebuth et al., 2011) but different to the islands of Tahiti (ca -28 m; Bard et al., 2010) and Barbados (ca -25 m; Peltier and Fairbanks, 2006). There are two

ways to interpret this: (i) the age of the lowermost SLIP in core Q7 is overestimated due to old carbon contamination of the dating material or, (ii) the relatively shallow shoreline position in our study area is a deviation from eustacy due to levering of the broad continental shelf in response to ocean load (e.g., Milne and Mitrovica, 2008). The similarity to the Sunda Shelf and absence of contamination elsewhere in the sediment cores suggests indeed that the broad-shelf effect (East China Sea shelf; Fig. 1) causes the shallow shoreline position. More SLIP data are needed to provide unequivocal evidence for it.

While SLIP data suggest a rising rate of ~0.4 cm/a during the early Holocene, the GIA models indicate ~0.5 cm/a (ICE-X) and ~0.9 cm/a (ANU). The ICE-X models approximate the observed early Holocene rising rate but the timing of this rise is offset by about 2000 years. In the ANU model the early Holocene sea level rises almost twice as fast as the observed one with an offset of ~500 years. Thus, the observed early Holocene sea level rises slower than the modelled sea level. For the mid-late Holocene SLIP data suggest ~0.04 cm/a rising rate while the GIA models indicate a falling sea level. Predictions obtained from ICE-5G and ICE-6G are generally relatively similar but deviate from each other in the timing of the mid-Holocene sea-level highstand. The GIA models, including BRAD, show the highstand (4.6 m -3.4 m; 0.5 m) at 7-6 ka while the SLIP data remain below modern sea level until 2 ka. The misfit between observed and predicted sea level rise is in the coastal zone south of Bohai Bay much smaller than in our study area (Fig. S3). This should reflect the geological structure of the area: our study area belongs to the North China Plain Subsidence Basin (Wang and Li, 1983), while the south of Bohai Bay lies on the edge of Shandong Upland (Fig.1b). Thus, the most -likely explanation for the Bohai Bay misfit is subsidence of the coastal plain. Subsidence is a non-GIA component and should become evident through the residuals (i.e. the difference between observation and prediction per unit of time; Fig. 7b). Indeed, we identify linearity of residuals for the period 7-0 ka, suggesting that subsidence dominates the local sea-level signal after the rise of the eustatic sea level has slowed down. A subsidence rate of 1.25 mm/a is estimated from the residuals, similar to Wang et al. (2003) who deduced a rate of ~1.5 mm/a from the 400-500 m thick Quaternary sequence in the bay. It is possible that fluvial sediment supply enhanced the subsidence rate in the Holocene. The Yellow River's annual discharge into Bohai Bay is estimated to 0.2 Gt until 740AD rising to 1.2 Gt until around 1800 when

widespread farming on the loess plateau started increasing the river's sediment load (Best, 2019). Thus, the sea-level rise in Bohai Bay is in the early Holocene dominated by the eustatic sea-level rise and GIA effects associated with the broad shelf from Bohai Sea to East China Sea, while in the mid-late Holocene it is dominated by a combination of tectonic subsidence and fluvial sediment load.

4. Conclusions

Using advanced methods for field survey and identification of accurate and precise sea-level markers, we have established a new Holocene sea-level history for central Bohai Bay. Our new data are not only different to previously published data in that they do not show the expected mid-Holocene sea level highstand, but they are also different to global GIA models. We see a possible broad-shelf effect elevating the shoreline by several meters in comparison to the tropical islands of Tahiti and Barbados and we see local processes controlling shoreline migration and coast evolution as soon as ice melting ceased. This indicates that more emphasis should be placed on regional coast and sea-level change modelling under a global sea-level rising future as the local government need more specific and effective advice to deal with coastal flooding.

5. ACKNOWLEDGMENTS

We thank one anonymous reviewer and Sarah Bradley for constructive suggestions on the manuscript. This work was supported by the China Geological Survey, CGS (DD20189506) and National Natural Science Foundation of China (Grant no. 41476074, 41806109, 41972196). The authors acknowledge PALSEA, a working group of the International Union for Quaternary Sciences (INQUA) and Past Global Changes (PAGES), which in turn received support from the Swiss Academy of Sciences and the Chinese Academy of Science.

References

Amante, C. and Eakins, B.: ETOPO1 Arc-Minute Global Relief Model: Procedures, Data Source and Analysis. Tech. rep, DOI: 10.7289/V5C8276M, 2009.

303 Bard, E., Hamelin, B. and Delanghe-Sabatier, D.: Deglacial meltwater pulse 1B and Younger Dryas sea
304 levels revisited with boreholes at Tahiti. Science, 327, 1235−1237. DOI: 10.1126/science.1180557, 2010.
305 Best, J.: Anthropogenic stresses on the world's big rivers. Nature Geoscience, 12, 7−21.
306 Doi:10.1038/s41561-018-0262-x, 2019.
307 Bradley, S.L., Milne, G.A., Horton, B.P., Zong, Y.Q.: Modelling sea level data from China and Malay-
308 Thailand to estimate Holocene ice-volume equivalent sea level change. Quaternary Science Reviews, 137,
309 54−68. DOI: 10.1016/j.quascirev.2016.02.002, 2016.
310 Brain, M.J. Chapter 30 Compaction. In: Shennan, I., Long, A.J., Horton, B.P. (Eds.): Handbook of Sea-level
311 Research. John Wiley & Sons Ltd. Chichester, UK, 2015.
312 Cang, S.X., Zhao, S.L., Zhang, H.C., Huang, Q.F.: Middle Pleistocene paleoecology, paleoclimatology and
313 paleogeography of the western coast of Bohai Gulf. Acta Palaeontologica Sinica 18(6): 579−591. DOI：
314 10.19800/j.cnki.aps.1979.06.006, 1979 (in Chinese with English abstract).
315 Farrell, W. and Clark, J.: On postglacial sea-level. Geophys. J. Roy. Astr. S., 46, 647–667. DOI:
316 10.1111/j.1365-246X.1976.tb01252.x, 1976
317 Feng, X.L., Lin, L., Zhuang, Z.Y, Pan, S.C.: The relationship between geotechnical paramenters and
318 sedimentary environment of soil layers since Holocene in modern Huanghe subaqueous Delta. Coastal
319 Engineering, 18, 4, 1−7. DOI: CNKI:SUN:HAGC.0.1999-04-000, 1999 (in Chinese with English abstract).
320 Geng, X.S.: Marine transgressions and regressions in east China since late Pleistocene Epoch. Acta
321 Oceanlogica Sinica, 3(1), 114−130.
322 http://www.hyxb.org.cn/aos/ch/reader/create_pdf.aspx?file_no=19810110&flag=&journal_id=aos&year_id
323 =1981, 1981 (in Chinese with English abstract).
324 Hanebuth, T.J.J., Voris, H.K., Yokoyama, Y., Saito, Y., Okuno, J.I.: Formation and fate of sedimentary
325 depocentres on Southeast Asia's Sunda Shelf over the past sea-level cycle and biogeographic implications.
326 Earth-Science Reviews, 104(1−3), 92−110. https://doi.org/10.1016/j.earscirev.2010.09.006, 2011.
327 He, Q.X.(Eds.): Marine Sedimentary Geology of China. Beijing: China Ocean Press: 464−466, 2006 (in
328 Chinese).

IPCC: Climate Change 2014: Synthesis Report. Contribution of Working Groups I, II and III to the Fifth Assessment Report of the Intergovernmental Panel on Climate Change [Core Writing Team, R.K. Pachauri and L.A. Meyer (eds.)]. IPCC, Geneva, Switzerland, 151 pp. https://www.ipcc.ch/report/ar5/syr/, 2014.

Lambeck, K., Purcell, A., Johnston, P., Nakada, M., Yokoyama, Y.: Water-load definition in the glacio-hydro-isostatic sea-level equation. Quaternary Science Reviews, 137, 54–68. DOI: 10.1016/s0277-3791(02)00142–7, 2003.

Li, J.F.; Kang, H.; Wang, H.; Pei, Y.D.; Modern geological action and discussion of influence facters on the west coast of Bohai Bay, China. Geological Survey and Research, 30(4), 295–301. http://www.tianjin.cgs.gov.cn/dzdcyyj/qkxz/20074/200801/P020160920812081540884.pdf, 2007 (in Chinese with English abstract).

Li, J., Pei, Y., Wang, F., Wang, H.: Distribution and environmental significance of living foraminiferal assemblages and taphocoenose in Tianjin intertidal zone, the west coast of Bohai Bay. Marine geology & Quaternary geology, 29(3), 9–21. DOI: CNKI:SUN:HYDZ.0.2009-03-004, 2009. (in Chinese with English abstract).

Li, J., Shang, Z., Wang, F., Chen, Y., Tian, L., Jiang, X., Wang, H.: Holocene sea level change on the west coast of the Bohai Bay. Quaternary Sciences, 35(2), 243–264. DOI: 10.11928/j.issn.1001-7410.2015.02.01, 2015 (in Chinese with English abstract).

Li, S.L.: Distribution of the foraminiferal thanatocoenosis of PEARL River estuary. Marine geology & Quaternary Geology, 5(2), 83–101. DOI：10.16562/j.cnki.0256-1492.1985.02.009, 1985 (in Chinese with English abstract).

Milne, G.A. and Mitrovica J.X.: Searching for eustasy in deglacial sea-level histories. Quaternary Science Reviews, 27, 2292–2302. DOI: 10.1016/j.quascirev.2008.08.018, 2008.Mitrovica, J. and Wahr, J.: Ice Age Earth Rotation. Annual Review of Earth and Planetary Sciences, 39, 577–616. DOI: 10.1146/annurev-earth-040610-133404, 2011.

Nakada, M. and Lambeck, K.: Glacial rebound and relative sea-level variations: a new appraisal. Geophysical Journal International, 90, 1, 171–224. DOI: 10.1111/j.1365-246X.1987.tb00680.x, 1987.

Nicholls, R.J. and Cazenave A.: Sea-level rise and its impact on coastal zones. Science, 328, 1517–1520. DOI: 10.1126/science.1185782, 2010.

Peltier, W.R.: Global glacial isostasy and the surface of the ice-age Earth: the ICE-5G (VM2) Model and GRACE, Annu. Rev. Earth Pl. Sc., 32, 111–149. https://doi.org/10.1146/annurev.earth.32.082503.144359, 2004.

Peltier, W.R., Drummond, R., and Roy, K.: Comment on Ocean mass from GRACE and glacial isostatic adjustment by DP Chambers et al., J. Geophys. Res.-Sol. Ea., 117, B11403. https://doi.org/10.1029/2011JB008967, 2012.

Peltier, W.R., and Fairbanks, R.G.: Global glacial ice volume and Last Glacial Maximum duration from an extended Barbados sea level record, Quat. Sci. Rev., 25(23), 3322–3337. DOI: 10.1016/j.quascirev.2006.04.010, 2006.

Qin, L., Shang, Z.W., Li, Y., Li, J.F.: Temporal and spatial distribution of the oyster reef in Biaokou to Zengkouhe area; Geological Survey and Research, 40(4), 306−310. http://www.tianjin.cgs.gov.cn/dzdcyyj/qkxz/20174/201802/P020180202566954723921.pdf, 2017 (in Chinese with English abstract).

Reimer, P.J., Bard, E., Bayliss, A., Beck, J.W., Blackwell, P.G., Ramsey, C.B., Buck, C.E., Cheng, H., Edwards, R.L., Friedrich, M., Grootes, P.M., Guilderson, T.P., Haflidason, H., Hajdas, I., Hatté, C., Heaton, T.J., Hogg, A.G., Hughen, K.A., Kaiser, K.F., Kromer, B., Manning, S.W., Niu, M., Reimer, R.W., Richards, D.A., Scott, E.M., Southon, J.R., Turney, C.S.M., van der Plicht, J.: IntCal13 and MARINE13 radiocarbon age calibration curves 0−50000 years cal BP. Radiocarbon, 55(4), 1869−1887. doi: 10.2458/azu_js_rc.55.16947Bronk Ramsey C and Lee S (2013), 2013.

Shang, Z.W., Wang, F., Li, J.F., Marshall, W.A., Chen, Y.S., Jiang, X.Y., Tian, L.Z., Wang, H.: New residence times of the Holocene reworked shells on the west coast of Bohai Bay, China. Journal of Asian Earth Sciences, 115, 492−506. DOI: 10.1016/j.jseaes.2015.10.008, 2016.

Shang, Z.W., Wang, F., Fang J., Li, J.F., Chen, Y.S., Jiang, X.Y., Tian, L.Z., Wang, H.: Radiocarbon ages of different fractions of peat on coastal lowland of Bohai Bay: marine influence? Journal of Oceanology and Limnology, https://doi.org/10.1007/s00343-019-7091-7, 2018.

Shennan, I., Long, A.J. and Horton, B.P.(Eds.): Handbook of sea-level research. Published by John Wiley & Sons, Ltd., 2015.

Spada, G. and Stocchi, P.: SELEN: a Fortran 90 program for solving the “Sea Level Equation”, Comput. Geosci., 33, 538–562. DOI: 10.1016/j.cageo.2006.08.006, 2007.

Spada, G. and Melini, D.: SELEN4 (SELEN version 4.0): a Fortran program for solving the gravitationally and topographically self-consistent sea-level equation in glacial isostatic adjustment modelling. Geoscientific Model Development, 12, 5055–5075. DOI: 10.5194/gmd-12-5055-2019, 2019

Su, S.W., Shang, Z.W., Wang, F., Wang, H.: Holocene Chenier: spatial and temporal distribution and sea level indicators in Bohai Bay. Geological Bulletin of China, 30(9), 1382−1395. DOI: 10.1007/s11589-011-0776-4, 2011(in Chinese with English abstract).

Tian, L.Z., Chen, Y.P., Jiang, X.Y., Wang, F., Pei, Y.D., Chen, Y.S., Shang, Z.W., Li, J.F., Li, Y., Wang, H.: Post-glacial sequence and sedimentation in the western Bohai Sea, China. Marine Gology, 388m 12–24. http://dx.doi.org/10.1016/j.margeo.2017.04.006, 2017.

Tegmark, M.: An icosahedron-based method for pixelizing the celestial sphere, Astrophys. J., 470, L81–L85, https://doi.org/10.1086/310310, 1996.

Wang, F., Li, J.F., Chen, Y.S., Fang, J., Zong, Y.Q., Shang, Z.W., Wang H.: The record of mid-Holocene maximum landward marine transgression in the west coast of Bohai Bay, China. Marine Geology, 359, 89−95. DOI: 10.1016/j.margeo.2014.11.013, 2015.

Wang, H., Chen, Y.S., Tian, L.Z., Li, J.F., Pei, Y.D., Wang, F., Shang, Z.W., Fan, C.F., Jiang, X.Y., Su, S.W., Wang, H.: Holocene cheniers and oyster reefs in Bohai Bay: palaeoclimate and sea level changes. Geological Bulletin of China, 30(9), 1405−1411. DOI: 10.1007/s11589-011-0776-4, 2011(in Chinese with English abstract).

Wang, P.X., Min, Q.B. and Bian, Y.H.: Distributions of foraminifera and ostracoda in bottom sediments of the northwestern part of the South Huanghai (Yellow) Sea and its geological significance. In: Wang, P. (Eds.), Marine Micropaleontology of China. China Ocean Press, Beijing, pp. 93−114, 1985 (in Chinese with English abstract).

Wang, P.X., Min, Q.B., Bian, Y.H., Cheng, X.R.: Strata of quaternary transgressions in east China: a preliminary study. Acta Geologica Sinica, 1, 1−13. DOI: 10.1007/BF01077538, 1981 (in Chinese with English abstract).

Wang, Q. and Li F.L.: The changes of marine-continental conditions in the west coast of the Bohai Gulf during Quaternary. Marine Geology&Quaternary Geology, 4, 83–89. DOI: 10.16562/j.cnki.0256-1492.1983.04.013, 1983 (in Chinese with English abstract).

Wang, R.B., Zhou, W., Li, F.L., Wang, H., Yang, G.Y., Yao, Z.J., Kuang, S.J.: Tectonic subsidence and prospect of ground subsidence control in Tianjin area. Hydrogeology & Engineering Geology, 5, 12−17. DOI: 10.1007/BF02873153, 2003 (in Chinese with English abstract).

Wang, Y.: The shell coast ridges and the old coastlines of the west coast of the Bohai Bay. Bulletin of Nanjing University (Edition of Natural Sciences), 8(3), 424–440. DOI: CNKI:SUN:NJDZ.0.1964-03-007, 1964 (with three plates) (in Chinese with English abstract).

Wang, Y.M.: A preliminary study on the Holocene transgression on the coastal plain along the north-western Bohai Bay. Geographical Research, 1(2), 59−69. DOI: 10.11821/yj1982020007, 1982 (in Chinese with English abstract).

Wang, Z., Zhuang, C., Staito, Y., Chen, J., Zhan, Q., Wang, X.: Early mid-Holocene sea-level change and coastal environmental response on the southern Yangtze delta plain, China: implications for the rise of Neolithic culture. Quaternary Science Reviews, 35, 51−62. DOI: 10.1016/j.quascirev.2012.01.005, 2012.

Wang, Z., Jones, B.G., Chen, T., Zhao, B., Zhan, Q.: A raised OIS3 sea level recorded in coastal sediments, southern Changjiang delta plain, China. Quaternary Research, 79, 424−438. DOI: 10.1016/j.yqres.2013.03.002, 2013.

Xiong, H., Zong, Y., Qian, P., Huang, G., Fu, S.: Holocene sea-level history of the northern coast of South China Sea. Quaternary Science Reviews 194, 12–26. https://doi.org/10.1016/j.quascirev.2018.06.022, 2018.

Xiong, H., Zong, Y., Li, T., Long, T., Huang, G., Fu, S.: Coastal GIA processes revealed by the early to middle Holocene sea-level history of east China. Quaternary Science Reviews, 233, 106249. DOI: 10.1016/j.quascirev.2020.106249, 2020.

Xue, C.T.: Historical changes in the Yellow River delta, China. Marine Geology 113, 321−329. DOI： 10.1016/0025-3227(93)90025-Q, 1993.

Yang, H.R. and Chen, Q.X.: Quaternary transgressions, eustatic changes and shifting of shoreline in east China. Marine Geology & Quaternary Geology, 5(4), 69−80. DOI：10.16562/j.cnki.0256-1492.1985.04.011, 1985 (in Chinese with English abstract).

Zhang, Y.C., Hu, J.J. and Liu, C.F.: Preliminary recognition of sea and land changes along the east coast of China since the terminal Pleistocene. Bulletin of the Chinese Academy of Geological Sciences, 19, 37−52. https://www.ixueshu.com/document/8e1a59a8c6fd86ca318947a18e7f9386.html, 1989 (in Chinese with English abstract).

Zhao, S.L., Yang, G.F., Cang, S.X., Zhang, H.C., Huang, Q.F., Xia, D.X., Wang, Y.J., Liu, F.S., Liu, C.F.: On the marine stratigraphy and coastlines of the western coast of the gulf of Bohai. Oceanologia Et Limnologia Sinica, 9(1), 15−25 http://qdhys.ijournal.cn/hyyhz/ch/reader/create_pdf.aspx?file_no=19780102&flag=&journal_id=hyyhz&year_id=1978, 1978 (in Chinese with English abstract).

Zhao, X.T., Geng, X.S., Zhang, J.W.: Sea level changes of the eastern China during the past 20000 years. Acta Oceanologia Sinica, 1(2), 269−281. http://www.hyxb.org.cn/aos/ch/reader/create_pdf.aspx?file_no=19790208&year_id=1979&quarter_id=2&flag=1, 1979.

Zong, Y.: Mid-Holocene sea-level highstand along the southeast coast of China. Quaternary International, 117, 55−67. DOI: 10.1016/S1040-6128(03)00116-2, 2004.

455 **Table 1. Analytical data used to establish SLIPs.**

Beta-lab code	Depth (m)	Altitude (m, msl)	Dated material	$\delta^{13}C$ (‰)	Conventional age (BP)	Calibrated age (BP) (2σ)	Median age (BP)	Indicative meaning and range	Sediment compaction (m)*	Palaeo-mean sea level
Core DC01										
329636	8.40	-4.66	Peat	-26.8	6950±40	7523-7430	7487	Terrestrial peat		
329637	9.27	-5.53	Bulk organic	-18.2	7410±60	8372-8153	8248	Terrestrial peat		
Core QX01										
329647	5.52	+0.36	Bulk organic	-22.5	4300±30	4892-4829	4343**	1.78±0.53	0.29±0.04	-1.14±0.57
329644	6.35	-1.19	Bulk organic	-23.6	5010±50	5900-5644	5226**	1.78±0.53	0.30±0.04	-2.68±0.57
329643	7.20	-2.04	Bulk organic	-25.0	5090±30	5912-5748	5288**	1.78±0.53	0.25±0.03	-3.58±0.56
329641	8.20	-3.04	Peat	-24.6	5830±30	6732-6554	6647	1.78±0.53	0.24±0.03	-4.58±0.56
329642	8.70	-3.54	Peat	-24.3	6030±40	6981-6778	6875	1.78±0.53	0.21±0.03	-5.11±0.56
329645	9.16	-4.00	Peat	-27.4	6220±40	7250-7006	7117	1.78±0.53	0.18±0.02	-5.60±0.55
329640	11.39	-6.23	Peat	-25.3	7010±30	7935-7786	7855	1.78±0.53	0.01±0.01	-8.00±0.54
329646	13.05	-7.89	Peat	-25.1	7200±30	8057-7952	8002	Terrestrial peat		
Core QX03										
353792	2.91	1.47	Peat	-20.6	2350±30	2461-2326	2357	Terrestrial peat		
353794	4.90	-0.42	Peat	-24.0	3390±30	3699-3569	3634	1.78±0.53	0.16±0.02	-2.01±0.55
353796	7.39	-3.01	Plant material	NA	5930±30	6799-6671	6752	1.78±0.53	0.10±0.02	-4.68±0.55
353798	8.63	-4.25	Plant material	-26.7	6410±40	7420-7271	7350	1.78±0.53	0.01±0.01	-6.02±0.54
353800	9.60	-5.22	Plant material	-28.2	6690±40	7622-7478	7562	Terrestrial peat		
353802	12.40	-8.02	Plant material	-28.3	7280±40	8429-8325	8397	Terrestrial peat		
Core QX02										

332798	3.65	-0.08	Bulk organic	-23.6	3680±30	4091-3913	3517**	1.78±0.53	0.30±0.04	-1.57±0.57
332792	5.68	-2.11	Bulk organic	-24.0	5450±30	6300-6204	5718**	1.78±0.53	0.36±0.04	-3.54±0.57
333329	7.27	-3.70	Peat	-26.7	6350±30	7331-7240	7283	1.78±0.53	0.32±0.04	-5.16±0.57
333330	8.98	-5.41	Peat	-26.3	6600±30	7522-7434	7494	1.78±0.53	0.19±0.02	-7.00±0.55
333331	10.97	-7.40	Peat	-27.2	7020±30	7934-7792	7867	Terrestrial peat		
333333	12.42	-8.85	Peat	-26.3	7140±40	8023-7925	7966	Terrestrial peat		
Core ZW15										
255821	1.6	0.03	Bulk organic	-22.5	2930±30	3168-2976	2584**	1.78±0.53	0.32±0.04	-1.44±0.57
356208	12.6	-10.97	Plant material	-25.0	7450±40	8358-8186	8271	1.78±0.53	0.00	-12.75±0.53
356209	13.5	-11.87	Plant material	-25.5	7640±40	8521-8381	8430	Terrestrial peat		
Core Q7										
358054	1.3	2.16	Bulk organic	-20.4	530±30	559-510	540	1.78±0.53	0.10±0.02	+0.49±0.55
357153	17.2	-13.74	Plant material	-28.0	7990±40	9005-8705	8868	1.78±0.53	0.16±0.02	-15.36±0.55
357157	18.85	-15.39	Bulk organic	-24.6	9140±40	10411-10226	9718**	1.78±0.53	0.00	-17.18±0.53
Core CZ01										
395014	15.42	-8.53	Peat	-27.5	8930±40	10099-9914	10047	Terrestrial peat		
Core CZ02										
395022	12.19	-6.42	Peat	-23.1	7950±30	8980-8648	8830	Terrestrial peat		
Core CZ03										
395026	4.42	-0.48	Bulk organic	-24.2	2730±30	2877-2762	2325**	1.78±0.53	0.12±0.02	-2.15±0.55
395027	6.15	-2.21	Peat	-25.1	4790±30	5593-5470	5517	1.78±0.53	0.19±0.02	-3.80±0.55
395028	6.54	-2.57	Bulk organic	-27.1	5830±30	6732-6554	6114**	1.78±0.53	0.18±0.03	-4.18±0.56
395029	7.51	-3.54	Peat	-26.7	6230±30	7251-7019	7167	1.78±0.53	0.14±0.02	-5.19±0.55
395030	9.22	-5.25	Peat	-27.3	6640±30	7576-7468	7528	1.78±0.53	0.01±0.01	-7.03±0.54

395031	9.34	-5.37	Peat	-20.0	6660±30	7583-7483	7535	1.78±0.53	0.00	-7.15±0.53
395032	10.23	-6.26	Peat	-27.2	6900±30	7794-7669	7726	Terrestrial peat		
395034	12.4	-8.43	Peat	-27.2	7290±30	8171-8025	8102	Terrestrial peat		
Core CZ87										
403413	2.66	1.8	Bulk organic	-20.8	2420±30	2696-2351	2446	Terrestrial peat		
403414	4.51	-0.05	Bulk organic	-23.8	3330±30	3637-3477	3566	Terrestrial peat		
406826	5.75	-1.29	Bulk organic	-24.1	4020±30	4536-4420	3970**	1.78±0.53	0.25±0.03	-2.83±0.56
403417	11.05	-6.59	Plant material	-27.9	6300±30	7275-7165	7223	1.78±0.53	0.04±0.01	-8.33±0.54
403418	12.62	-8.16	Plant material	-27.6	6990±30	7876-7736	7829	Terrestrial peat		
Core CZ61										
407339	2.52	1.24	Bulk organic	-20.8	2310±30	2359-2306	2337	Terrestrial peat		
406823	4.72	-0.96	Plant material	NA	2780±30	2952-2793	2877	1.78±0.53	0.16±0.02	-2.58±0.55
406824	6.20	-2.44	Bulk organic	-23.9	6100±30	7029-6884	6433**	1.78±0.53	0.25±0.03	-3.98±0.56
403397	9.73	-5.97	Plant material	-19.6	6760±30	7664-7577	7615	1.78±0.53	0.00	-7.75±0.53
403398	11.04	-7.37	Plant material	-27.5	7000±30	7932-7756	7842	Terrestrial peat		
403399	12.90	-9.14	Plant material	-28.0	7160±30	8018-7939	7980	Terrestrial peat		
Core CZ65										
399705	4.93	-1.97	Bulk organic	-18.5	3920±30	4428-4280	3397	Terrestrial peat		
399708	9.58	-6.62	Plant material	-27.2	7000±30	7883-7756	7823	1.78±0.53	0.01±0.01	-8.39±0.54
399710	11.50	-8.54	Plant material	-27.1	7250±30	8162-8001	8080	Terrestrial peat		
Core CZ80										
403401	3.73	2.69	Bulk organic	-20.3	3170±30	3452-3346	3400	Terrestrial peat		
403403	6.57	-0.15	Bulk organic	-22.1	5050±30	5901-5726	5298	1.78±0.53	0.20±0.03	-1.74±0.56
406825	8.75	-2.33	Peat	NA	5840±30	6736-6562	6660	1.78±0.53	0.09±0.01	-4.02±0.54

403408	11.53	-5.11	Plant material	-27.5	6450±30	7428-7313	7370	Terrestrial peat		
403409	12.05	-5.63	Plant material	-27.9	6610±30	7565-7440	7503	Terrestrial peat		
403410	12.34	-5.92	Plant material	-26.4	6860±30	7759-7618	7687	Terrestrial peat		
403411	13.84	-7.42	Plant material	-24.6	7300±30	8175-8029	8105	Terrestrial peat		
Core CZ85										
399719	3.67	0.94	Bulk organic	-20.5	3460±30	3671-3641	3225**	1.78±0.53	0.17±0.03	-0.68±0.56
399720	6.77	-2.16	Bulk organic	-25.4	5830±30	6732-6554	6114**	1.78±0.53	0.08±0.01	-3.87±0.54
399721	8.33	-3.72	Plant material	-26.4	6020±30	6947-6785	6862	1.78±0.53	0.01±0.01	-5.49±0.54
399722	12.70	-8.09	Plant material	-28.0	7270±30	8165-8015	8096	Terrestrial peat		
Core CZ66										
399712	3.62	0.25	Bulk organic	-23.4	3930±30	4440-4282	3856**	1.78±0.53	0.32±0.04	-1.22±0.57
399713	5.21	-1.34	Bulk organic	-25.1	5730±30	6632-6445	5992**	1.78±0.53	0.39±0.05	-2.74±0.58
399714	8.14	-4.27	Plant material	-27.4	6710±30	7651-7510	7581	1.78±0.53	0.24±0.03	-5.81±0.56
399715	10.03	-6.16	Plant material	-26.6	6790±30	7675-7587	7635	1.78±0.53	0.08±0.01	-7.86±0.54
399716	12.49	-8.62	Plant material	-27.1	7220±30	8156-7965	8021	Terrestrial peat		
399718	13.63	-9.76	Plant material	-27.6	7670±30	8523-8406	8452	Terrestrial peat		

s* Sediment compaction = 10% of compressible thickness divided by lapse time of deposition in the past 9000 years

** corrected for marine influence on salt marsh organic sample fraction ages of peaty clay

459 **Figure captions**

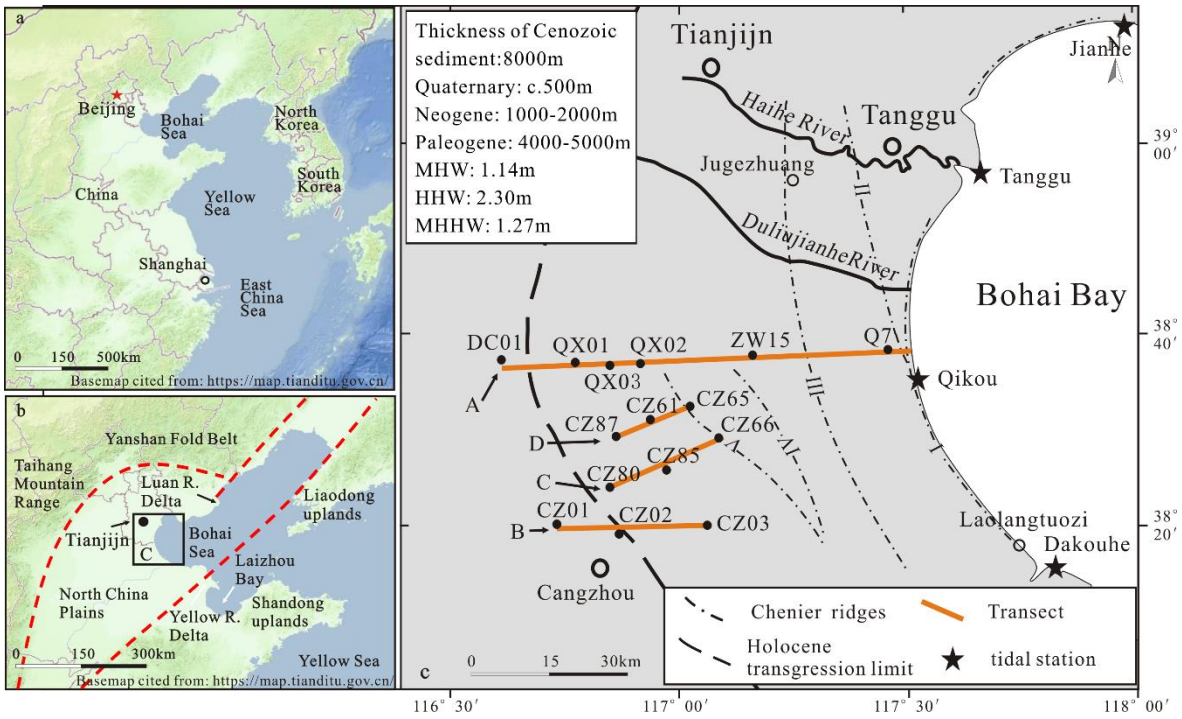

460
461

462 **Figure 1. The study area; (a) location of Bohai Bay and Yellow Sea; (b) location of the study area and major river**

463 **deltas; red dashed lines indicate the topographic boundaries of coastal lowland, (c) locations of boreholes,**

464 **transects A, B, C, D, Chenier ridges (Su et al. (2011; Wang et al., 2011) and Holocene transgression limit (Xue,**

465 **1993). The basemap of Fig.1a and Fig.1b are cited from "map world" (https://www.tianditu.gov.cn/, National**

466 **Plateform for Common Geispatial Information Services, China)**

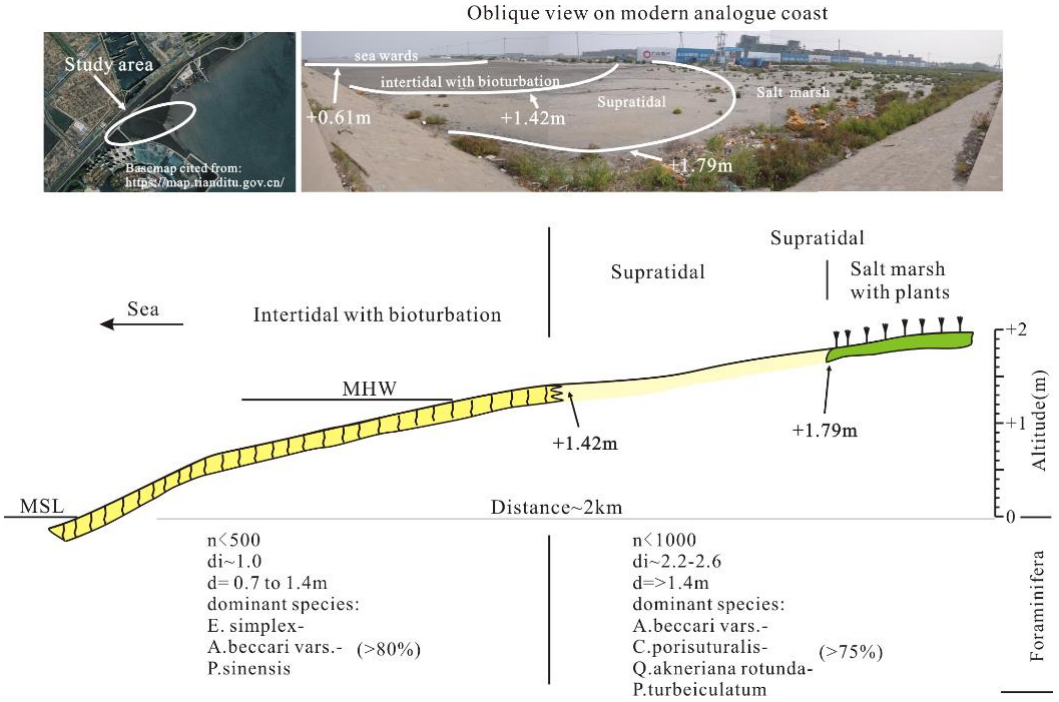

467

468 **Figure 2. Schematic cross-section of the modern tidal flat of the study area showing two characteristic**

469 **foraminiferal zones. The basemap of study area is derived from "map world" (https://www.tianditu.gov.cn/,**

470 **National Plateform for Common Geispatial Information Services, China)**

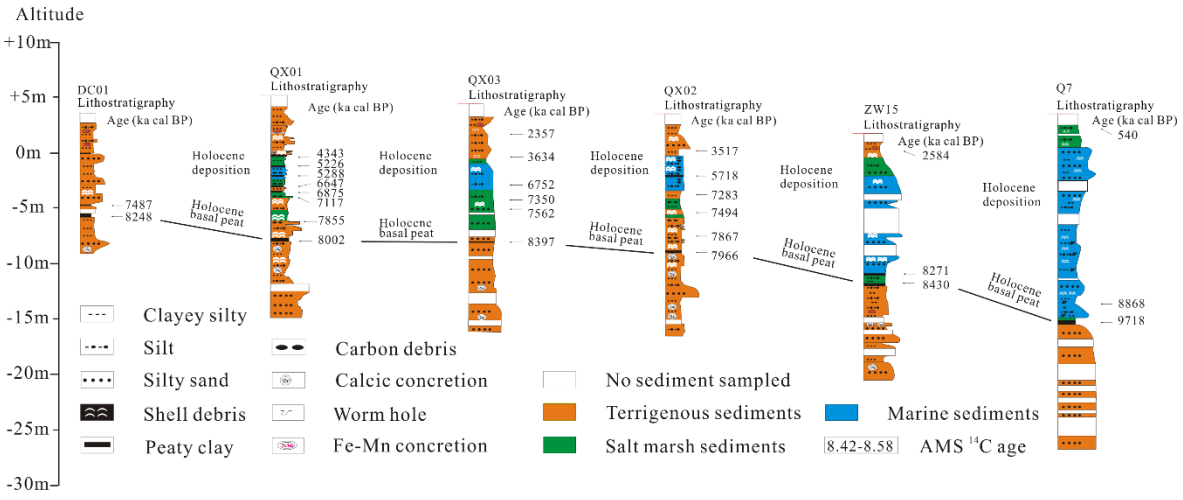

471

472 **Figure 3. The lithostratigraphy of transect A, with details of dated sedimentary horizons.**

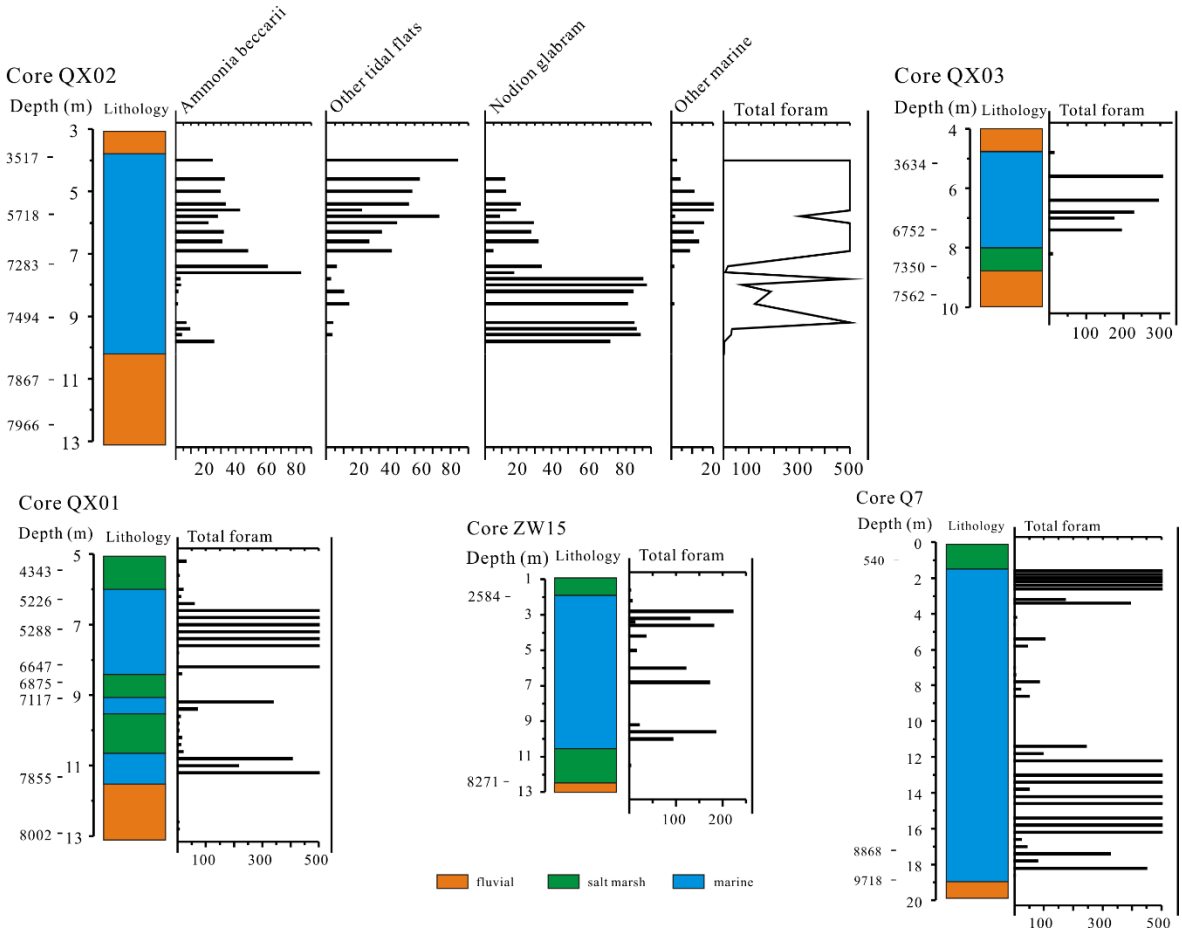

473

474 **Figure 4. Foraminiferal counts from five cores of transect A. Counts > 500 are shown as 500.**

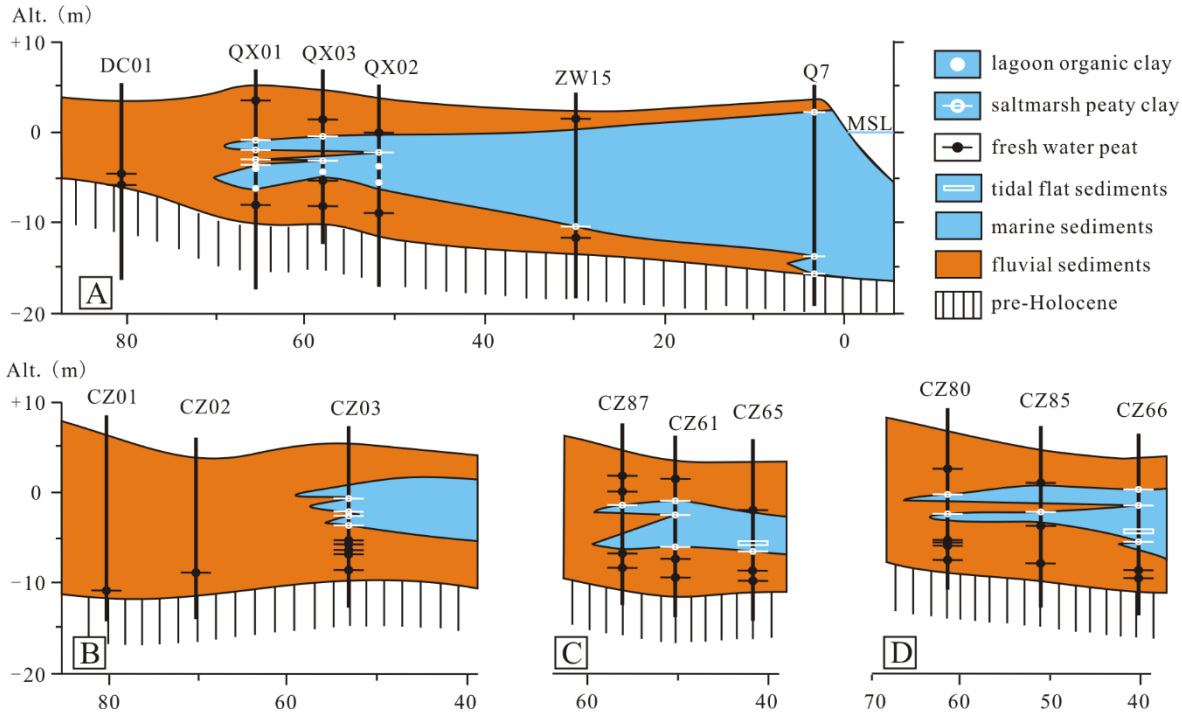

475

476 **Figure 5. The lithostratigraphy of transects B, C and D, with details of dated sedimentary horizons.**

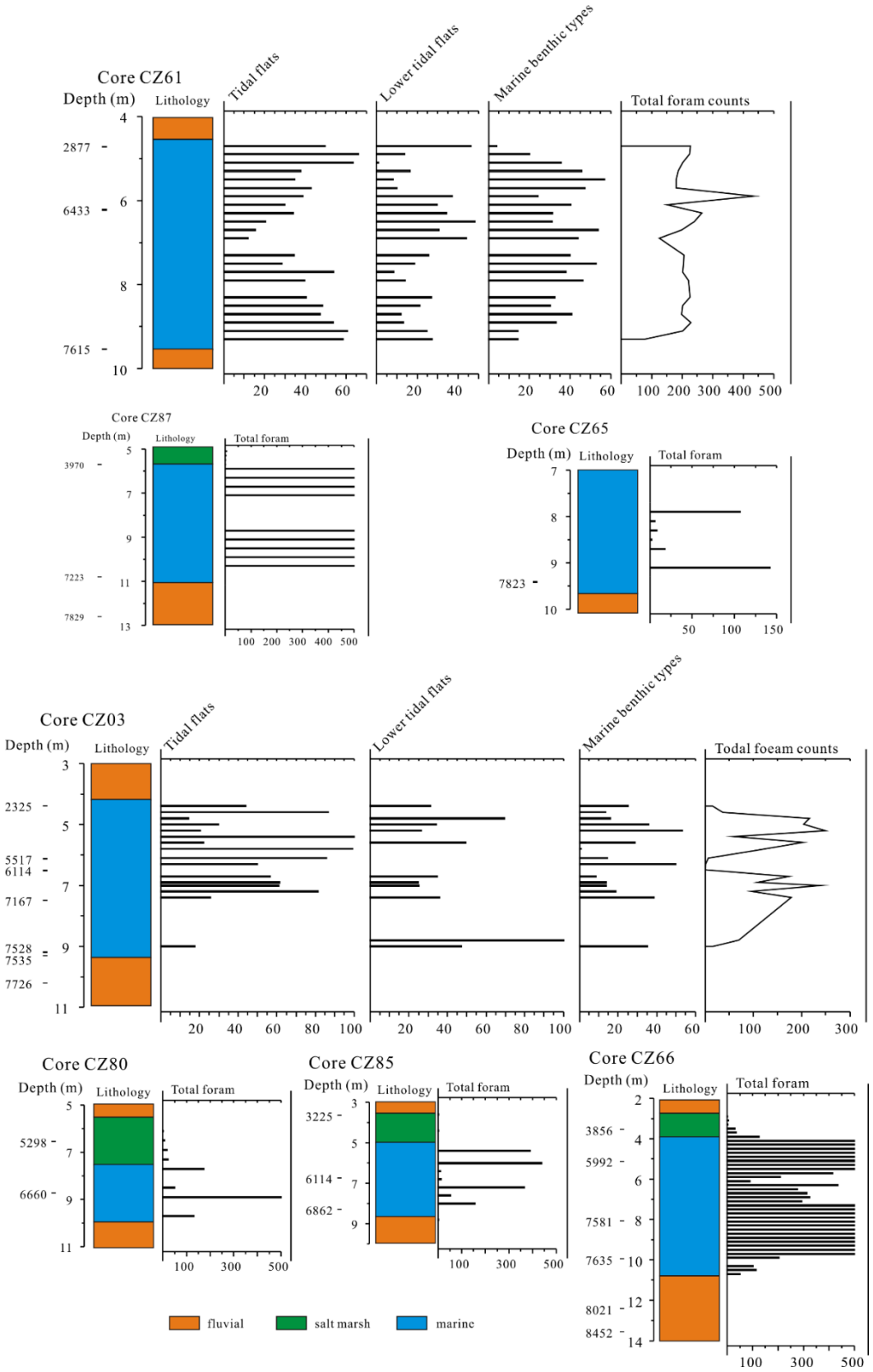

Figure 6. Foraminiferal counts from five cores of transects B, C and D. Counts > 500 foraminifera are shown as 500.

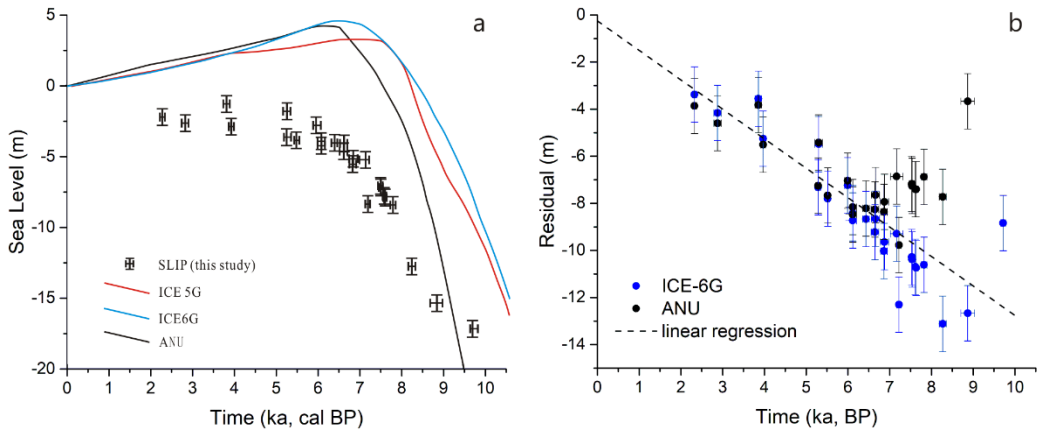

Figure 7. Observed and predicted sea level in Bohai Bay and resulting residuals; (a) SLIPs generated in this study and sea-level predictions. ICE-5G, ICE-6G and ANU are GIA models described in section 3.6. Lithospheric thickness (km): 65 (ANU), 90 (5G and 6G); upper mantle viscosity (Pa s) = 0.5×10^{21} (ANU, 5G, 6G); lower mantle viscosity (Pa s): 10×10^{21} (ANU), 2.7×10^{21} (5G), 3.2×10^{21} (6G); see also Table S1; age error bars are too small to be clearly visible. (b) Sea-level residuals plotted against time. Residuals are the difference between SLIPs and interpolated model data points. Error bars are derived from SLIP uncertainties. The trend line (dashed line) is computed as a least-squares regression on the mean residuals obtained with ANU and ICE-6G. The regression line approximates zero elevation remarkably closely which gives confidence that the calculated 1.25 mm/a for the non-GIA component is correct.

491 Author contribution

Author name	Contributions
Fu Wang	Scientific questions choice, design of field work including sampling andmeasurements, data analyses, results and discussion, paper writing and revising.
Yongqiang Zong	Revise part of the paper and English writing check.
Barbara Mauz	Revise part of the paper and English writing check.
Jianfen Li	Sampling and foraminifera analysis.
Jing Fang	Sampling and foraminifera analysis.
Lizhu Tian	Sampling and foraminifera analysis.
Yongsheng Chen	Sampling and foraminifera analysis.
Zhiwen Shang	Sampling and foraminifera analysis.
Xingyu Jiang	Sampling and foraminifera analysis.
Giorgio Spada	GIA model work and writing sec 3.6
Daniele Melini	GIA model work and residual calculation

492